

# Wilson-Bappu Effect: Extended to Surface Gravity

Sunkyung Park<sup>1</sup>, Wonseok Kang<sup>1</sup>, Jeong-Eun Lee<sup>1</sup>, Sang-Gak Lee<sup>2</sup>

<sup>1</sup> School of Space Research, Kyung Hee University, Yongin-Si, Gyeonggi-Do 446-701, Republic of Korea; sunkyung@khu.ac.kr, wskang@khu.ac.kr, jeongeun.lee@khu.ac.kr

<sup>2</sup> Astronomy Program, Department of Physics and Astronomy, Seoul National University, Seoul 151-742, Republic of Korea; sanggak@snu.ac.kr

Received \_\_\_\_\_; accepted \_\_\_\_\_

## ABSTRACT

Wilson and Bappu found a tight correlation between the stellar absolute visual magnitude ( $M_V$ ) and the width of the Ca II K emission line for late-type stars in 1957. Here, we revisit the Wilson-Bappu relationship (hereafter, WBR) to claim that WBR can be an excellent indicator of stellar surface gravity of late-type stars as well as a distance indicator. We have measured the width ( $W$ ) of the Ca II K emission line in high resolution spectra of 125 late-type stars, which were obtained with Bohyunsan Optical Echelle Spectrograph (BOES) and adopted from the UVES archive. Based on our measurement of the emission line width ( $W$ ), we have obtained a WBR of  $M_V = 33.76 - 18.08 \log W$ . In order to extend the WBR to be a surface gravity indicator, the stellar atmospheric parameters such as effective temperature ( $T_{\text{eff}}$ ), surface gravity ( $\log g$ ), metallicity ( $[\text{Fe}/\text{H}]$ ), and micro-turbulence ( $\xi_{\text{tur}}$ ) have been derived from the self-consistent detailed analysis using the Kurucz stellar atmospheric model and the abundance analysis code, MOOG. Using these stellar parameters and  $\log W$ , we found that  $\log g = -5.85 \log W + 9.97 \log T_{\text{eff}} - 23.48$  for late-type stars.

*Subject headings:* Stars: late-type — Stars: fundamental parameters — Techniques: spectroscopic

## 1. Introduction

The Ca II K line ( $\lambda = 3933.7 \text{ \AA}$ ) of late-type stars has chromospheric emission feature superimposed on the deep photospheric absorption. The Ca II K emission feature is stronger in more evolved stars since the chromospheric activity increases as a late-type star evolves from the main sequence to the giant stages (i.e., as the luminosity increases) (Pasquini et al. 1990; Dupree et al. 1999).

Wilson & Bappu (1957) found a strong relationship between the absolute visual magnitude ( $M_V$ ) and the width of the Ca II K emission line ( $\log W$ ) of late-type stars, referred to as the Wilson-Bappu relation (WBR); one feature of this relation is that it is independent of stellar spectral type. Wallerstein et al. (1999) obtained the WBR using *Hipparcos* parallaxes for the first time. Pace et al. (2003) used high resolution spectra and *Hipparcos* data to obtain a WBR, and they applied the WBR to estimate the distance to M67.

Several studies regarding the relationship between the width of the Ca II K emission line and the stellar parameters, such as effective temperature ( $T_{\text{eff}}$ ), surface gravity ( $\log g$ ), and metallicity ( $[\text{Fe}/\text{H}]$ ) have been carried out over the past four decades (Reimers 1973; Neckel 1974; Ayres 1979; Lutz & Pagel 1982). Reimers (1973) found empirically that the width of the Ca II K emission line is related to  $T_{\text{eff}}$  and  $\log g$  and Neckel (1974) provided a theoretical framework for this relation. Ayres (1979) showed how the width of the Ca II K emission line varies with the surface gravity ( $\Delta\lambda_{HWHM} \sim g^{-1.4}$ ) and  $T_{\text{eff}}$ ; the width is sensitive to the gravity, but insensitive to  $T_{\text{eff}}$ . Lutz & Pagel (1982) also showed that the width of the Ca II K emission line depends on  $T_{\text{eff}}$ ,  $\log g$ , and  $[\text{Fe}/\text{H}]$ . Dupree & Smith (1995) also reported that the width of the Ca II K emission line depends on  $[\text{Fe}/\text{H}]$  in

---

<sup>1</sup>Corresponding Author : Jeong-Eun Lee (jeongeun.lee@khu.ac.kr)

metal-poor stars with  $[\text{Fe}/\text{H}] = -2 \sim -3$ . However, Gomez et al. (2012) re-examined the dependence of  $[\text{Fe}/\text{H}]$  on WBR and they concluded that WBR is insensitive to metallicity.

Recently, late-type stars, especially M dwarfs, have been a subject of interest because planets in the habitable zone can be more easily detected in late-type (low-mass) stars. The chemical composition of host stars is an important connection between the properties of planets and the environment in which they formed. Conventionally, the chemical abundances of late-type stars are estimated using an abundance analysis code and a model stellar atmosphere, which requires the information of  $T_{\text{eff}}$ ,  $\log g$ , and  $[\text{Fe}/\text{H}]$ . However, stellar atmospheric models require spectra covering a sufficient number of Fe I and Fe II lines. In addition, singly ionized atomic absorption lines such as Fe II are not easily detected in M type stars, including M dwarfs.  $T_{\text{eff}}$  of late-type stars can be derived relatively easily using spectroscopic or photometric methods (e.g. van Belle et al. 1999; Casagrande 2010). However, a simple indicator of stellar gravity has not yet been proposed.

In this context, we extend WBR to be an indicator of the surface gravities of late-type stars, including M type stars. This is done for the first time, although there have been many studies regarding WBR over the half-century.

In Section 2, we describe our observations and spectral data. In Section 3, we explain our method for determining the parameters of stellar atmospheres and measuring the width of the observed Ca II K emission lines. We present our results and discuss WBR as a surface gravity indicator, in Sections 4 and 5, respectively. We summarize our results in Section 6.

## 2. The Data

### 2.1. BOES Observations

The Bohyunsan Optical Echelle Spectrograph (BOES) is a high resolution echelle spectrograph attached to a 1.8-m optical telescope at Bohyunsan Optical Astronomy Observatory (BOAO). 41 G and K type stars were observed using BOES in 2008 and 2009 (Kang et al. 2011) and 31 G, K and M type stars were observed during April 2-5 and May 21-23 in 2012 at spectral resolution ( $R = \frac{\lambda}{\Delta\lambda}$ ) of 45,000 using the 200  $\mu\text{m}$  fiber. The observed wavelength range was 3600Å – 10500Å, covering the full optical spectrum. The signal-to-noise ratio (SNR) at the bottom of the Ca II K emission line is typically about 30, ranging from 12 to 107. The information on the observed targets are listed in Table 1.

The observation data were reduced by the IRAF (Image Reduction and Analysis Facility) `echelle` package. Each aperture from the spectral images was extracted using a master flatfield image. Using the flatfielding process, we corrected the interference fringes and pixel-to-pixel variations of the spectrum images. A ThAr lamp spectrum was used for wavelength calibration.

### 2.2. UVES Archive

Echelle spectra of 53 late-type stars (G, K and M) were adopted from the UVES POP (Paranal Observatory Project) field star archive (Bagnulo et al. 2003). UVES POP provides data in a reduced form. The spectra were obtained using the UVES echelle spectrograph at the Very Large Telescope (VLT) by the European Southern Observatory (ESO). To cover the full optical wavelength range (304 – 1040 nm), all stars were observed with two instrument modes: Dichroic #1 and Dichroic #2. We used the Dichroic #2 437 blue arm data, which has a central wavelength of 437 nm and covers 373 to 499 nm, where the Ca II

K emission line is located.

UVES provides high resolution and efficiency at UV wavelengths. The UVES data have a spectral resolution of  $\sim 80,000$  and median SNR of  $\sim 100$  at the bottom of the Ca II K emission line; the SNR of the UVES spectra ranges from 32 – 246. The stars included in this work are listed in Table 1.

### 3. Spectroscopic Analysis

#### 3.1. Stellar Atmospheric Parameters

By using a model atmosphere and abundance analysis code, we determined  $T_{\text{eff}}$ ,  $\log g$ , [Fe/H] and micro-turbulence ( $\xi_{\text{tur}}$ ) for the stellar atmosphere. We performed a self-consistent detailed analysis using the equivalent widths ( $EWs$ ) of the Fe I and Fe II lines. The  $EWs$  of the Fe I and Fe II lines were measured using TAME (Tool for Automatic Measurement of Equivalent-width) (Kang & Lee 2012) for the 80 G and K type stars, whose stellar properties are appropriate to use the adopted stellar atmospheric model (e.g.  $T_{\text{eff}} \geq 3500$  K). From the  $EWs$  data, the Fe abundance from each Fe I and Fe II line was estimated by the revised 2010 version of MOOG (Snedden 1973) and Kurucz ATLAS9 model grids (Kurucz 1993).

We chose the effective temperature and the micro-turbulence that minimized the slope of [Fe/H] derived from the individual lines as a function of, respectively, the excitation potentials (EP) and the  $EWs$  of the lines. Then we chose the surface gravity that minimized the difference between iron abundances derived from Fe I and Fe II lines (“ $\log g_{\text{model}}$ ” is used to refer to the gravity derived by the stellar atmospheric model hereafter). We selected the average of the Fe abundances derived from the Fe I and Fe II analysis as the metallicity. The method is iterative (find more details in Kang et al. 2011). We iterated until the

slopes of Fe I abundance vs. EP and  $EW$  become smaller than  $10^{-5}$ , and the difference between the abundances from Fe I lines and from Fe II lines becomes smaller than 0.003 dex. Through this procedure, we determined the final stellar atmospheric parameters of the 80 G and K type stars, and their stellar atmospheric parameters are listed in Table 1.

### 3.2. Measurement of the Emission Width of a Ca II K Line

In the past, both Ca II H and K lines were used to derive WBR because of the low spectral resolution. However, in high resolution spectroscopy, it has been revealed that the Ca II H line is contaminated by other adjacent lines, and thus only the Ca II K line can be used for WBR (Wilson 1976). Hence, we also used Ca II K emission line widths to derive the WBR of our samples.

We measured the widths of the Ca II K emission lines for our samples using the method from Pasquini (1992), Dupree & Smith (1995), and Pace et al. (2003). The width of the Ca II K emission line is defined as the wavelength difference between the half intensities of two emission peaks (dashed lines in Fig. 1). The widths calculated by this method show better correlation between  $M_V$  and  $\log W$  than those of Wilson’s method, which uses the wavelength difference between two minimum points. We define the errors of the line widths (1) as the standard deviation for the stars observed more than three times or (2) as the half difference between the largest and the smallest values measured for the stars with 2 or 3 spectra. The UVES data are observed at least twice. However, only three stars were observed more than once with BOES. Therefore, for the three stars, we applied the same method as used for the UVES data. Then, the average value of the three errors was adopted for the stars observed with BOES only once. Measured widths of the Ca II K emission lines are listed in Table 1.

Lutz (1970) defined  $W_0$  as the width at half-maximum of the emission profile, with a correction applied to account for the resolution limit of the spectrograph itself, which may broaden the lines. Dupree & Smith (1995) and Pace et al. (2003) did not correct for instrumental broadening because this effect was much smaller than the observed line width of the emission component. The predicted width of the BOES instrumental profile is about  $0.1 \text{ \AA}$ , which we estimated from the emission lines in the comparison lamp spectrum and is  $5 \sim 28 \%$  of the line widths of the Ca II K emission line of our samples (the median value is  $\sim 15 \%$ ). The width of the UVES instrumental profile is about  $0.15 \sim 0.20 \text{ \AA}$  (Cox et al. 2005), but the data are provided as a reduced form, which are almost free from the instrumental profile. As a result, we ignore the instrumental broadening effect following Dupree & Smith (1995).

## 4. Results

### 4.1. The Wilson-Bappu Relation

The absolute visual magnitudes ( $M_V$ ) were calculated from apparent visual magnitudes ( $m_V$ ) and trigonometric parallaxes, both of which are taken from the *Hipparcos* Catalogue (van Leeuwen 2007). In order to minimize the absolute magnitude error, the samples were limited to stars which have parallax errors less than 10%. As a result, 125 stars were selected, and are listed in Table 1, along with their calculated absolute magnitudes.

Using  $M_V$  and the width of the Ca II K emission line ( $\log W$ ) (Table 1), we obtained the WBR by a linear least squares fit weighting of the  $M_V$  errors. In this fitting, we considered the Lutz-Kelker effect; Lutz & Kelker (1973) noted that there is a systematic error in absolute magnitude as the observed parallaxes are larger than the true parallaxes on average. This systematic error is related to the ratio of parallax error to parallax ( $\frac{\sigma_\pi}{\pi}$ )



(see Table 1 in Lutz & Kelker (1973) or Table 3 in this paper). 104 stars in our samples have  $\frac{\sigma_\pi}{\pi}$  less than 0.050 indicating that the correction for  $M_V$  is  $\sim 0.02$  mag. Only 8 stars in our samples have  $\frac{\sigma_\pi}{\pi}$  larger than 0.075, for which 0.11 mag must be applied to correct for  $M_V$ . As a result, our WBR is

$$M_V = 33.76 - 18.08 \log W, \quad (1)$$

as shown in Fig. 2.  $M_V$  and  $\log W$  show a very tight correlation, with a Pearson’s correlation coefficient of 0.98, and the standard deviation is 0.66.

Extinction can affect the absolute magnitudes of stars. However, the distance to most of our sources (114 stars) is less than 200 pc. When we used only the 114 stars within 200 pc to minimize the extinction effect as in Pace et al. (2003), the derived WBR was not very different (0.03 mag) from our original WBR (Eq. (1)).

We also examined the effect of metallicity in our WBR. The metallicity of our samples covers a wide range ( $-0.72 \leq [\text{Fe}/\text{H}] \leq 0.42$ ), although the majority of our sources are close to solar metallicity (Fig. 3). The correlation coefficient between (O-C)M<sub>v</sub>, which is the difference in M<sub>v</sub> between the observed data point and the linear fit, and [Fe/H] is 0.49 for all of our sources, and it is 0.29 for the stars that have metallicity smaller than 0.0. Therefore, we conclude that there is no metallicity dependence of the WBR in our sample, as noted in previous studies (Wilson & Bappu 1957; Gomez et al. 2012).

In order to evaluate our measurements, we compared our  $W$ s with those in previous studies by Pace et al. (2003) and Wallerstein et al. (1999). The data used in Pace et al. (2003) were obtained under very similar conditions to our sample; they used high resolution spectra ( $R \sim 60,000$ ), parallaxes and visual magnitudes from the *Hipparcos* Catalogue (ESA 1997), and same definition of the width of the Ca II K emission line. However, the data from Wallerstein et al. (1999) were obtained under different conditions from ours; they used *Hipparcos* parallaxes (ESA 1997) and Ca II K emission line width adopted from

Wilson (1976), where  $W_0 = W - 18$  [km/s], taking into account the instrumental width.

We have 14 and 28 stars in common with Pace et al. (2003) and Wallerstein et al. (1999), respectively. The mean differences of  $W$  between our measurements and their values are  $\sim 0.02$  Å and  $0.10$  Å, and the standard deviations are  $\sim 0.06$  Å and  $0.11$  Å, respectively, as seen in Fig. 4. The relations between our widths and those measured by Pace et al. (2003) or Wallerstein et al. (1999) have slopes equal to 1 within the errors. Therefore, we corrected widths from Pace et al. (2003) and Wallerstein et al. (1999) by subtracting the intercept value of  $-0.05$  Å and  $-0.10$  Å found in Fig. 4 to make a homogeneous data sample when combined with ours. We included 131 stars from Pace et al. (2003) and 326 stars from Wallerstein et al. (1999), which are not in our list and have parallax errors smaller than 10%. We calculated  $M_V$  for these 457 stars using *Hipparcos* Catalogue (van Leeuwen 2007) for data homogeneity. As a result, we obtained the WBR from the 582 stars as  $M_V = 34.41 - 18.38 \log W$  (dashed line in Fig. 5). The median difference is about 0.20 between  $M_V$  calculated by our WBR (125 stars) and the WBR with the extended sample (582 stars). Therefore, this test supports that our WBR is well-calibrated.

## 4.2. Emission Width as a Surface Gravity Indicator

$\log W$  has a tight relationship (WBR) with  $M_V$ , which is associated with effective temperature and stellar radius;  $M_V \propto \log L \propto \log(R_*^2 T_{eff}^4) \propto \log(M_* g^{-1} T_{eff}^4) = \log M_* - \log g + 4 \log T_{eff}$ , where  $M_*$  is the stellar mass. As a result, because  $L \propto M_*^\gamma$ ,  $M_V \propto \log W \propto \log L \propto \alpha \log g + \beta \log T_{eff}$ , where  $W$  is the width of the Ca II K emission line. Hence, we revisit WBR in order to derive the surface gravities of late-type stars based on homogeneous high spectral resolution observations, using a consistent analysis across the sample.

Using 80 G and K type stars with determined atmospheric parameters, first, we derived the relation between the width of the Ca II K emission line ( $\log W$ ) and surface gravity ( $\log g_{\text{model}}$ ) as  $\log g_{\text{fit}} = 16.88 - 7.85 \log W$  (Fig. 6). However, as expected,  $\log W$  varies with temperature at a given gravity, as seen for  $\log g_{\text{model}} > 4.0$  in Fig. 6 (a smaller  $\log W$  at a lower temperature). Therefore, we take into account  $T_{\text{eff}}$  in order to determine the relationship between  $\log g_{\text{model}}$  and  $\log W$ .

From a linear regression analysis of  $\log g_{\text{model}}$  with  $\log W$  and  $\log T_{\text{eff}}$ , we found that  $\log g_{\text{fit}}$  has the following strong relationship with  $\log W$  and  $\log T_{\text{eff}}$ ,

$$\log g_{\text{fit}} = -5.85 \log W + 9.97 \log T_{\text{eff}} - 23.48. \quad (2)$$

Fig. 7 shows the relation between the model-determined surface gravity,  $\log g_{\text{model}}$ , and the surface gravity estimated by Eq. (2),  $\log g_{\text{fit}}$ . The standard deviation of the differences between  $\log g_{\text{model}}$  and  $\log g_{\text{fit}}$  is 0.21 dex.

Therefore, Eq. (2) can be used directly in order to estimate the stellar surface gravity of a late-type star within this uncertainty when the width of the Ca II K emission line is measured, and the effective temperature of the star is known.

## 5. Discussion

### 5.1. Application of WBR to the Distance

WBR can be used as a distance indicator since the absolute visual magnitude can be calculated with the Ca II K emission line width. We applied our WBR to the open cluster M67 in order to calculate its distance modulus by using the spectra in Dupree et al. (1999). Dupree et al. (1999) used Ca II H & K emission lines with intermediate resolution ( $R \sim 30,000$ ) echelle spectra of 15 red giants in M67. We have adopted 5 of the best quality

spectra (Sanders ID numbers : 978, 1016, 1221, 1250, 1479), shown in Fig. 8. As noted in Pace et al. (2003), we could not find the apparent Ca II K emission lines from the following Sanders ID numbers : 258, 989, 1279, and 1316. The comparison between our results and those of Pace et al. (2003) is listed in Table 2.

Based on their WBR, Pace et al. (2003) calculated the average distance modulus of M67 as 9.65 mag ( $\pm 0.2$  mag). In previous studies (Montgomery et al. 1993; Carraro 1996; Sarajedini et al. 2009), the range of the average of M67 is  $9.55 \leq (m - M)_V \leq 9.85$  mag.

To estimate the distance modulus to M67 using our WBR ( $M_V = 33.76 - 18.08 \log W$ ), we measured the widths of the Ca II K emission lines for the 5 stars listed above. The absolute magnitudes of the stars calculated with our WBR are listed in Table 2. The mean distance modulus of the 5 stars is 9.86, which is similar to 9.90, the mean distance modulus of the same 5 stars calculated by Pace et al. (2003). Our distance modulus also agrees well with values derived in previous studies (Montgomery et al. 1993; Carraro 1996; Sarajedini et al. 2009).

## 5.2. Comparison with Lutz & Pagel (1982)

Lutz & Pagel (1982) suggested that the width of the Ca II K emission line is related to stellar metallicity ( $[\text{Fe}/\text{H}]$ ) as well as  $\log g$  and  $T_{\text{eff}}$ . Although the majority of our stars are comparable to the solar metallicity, our full sample spans a wide range of metallicity ( $-0.72 \leq [\text{Fe}/\text{H}] \leq 0.42$ ). If we fit  $\log W$  with all three stellar parameters ( $\log g$ ,  $T_{\text{eff}}$ , and  $[\text{Fe}/\text{H}]$ ), the obtained relation is

$$\log g_{[\text{Fe}/\text{H}]} = -5.91 \log W + 9.40 \log T_{\text{eff}} + 0.46[\text{Fe}/\text{H}] - 21.25. \quad (3)$$

The metallicity term ( $0.46[\text{Fe}/\text{H}]$ ) is significantly smaller than those of the width ( $5.91 \log W$ ) and the temperature ( $9.40 T_{\text{eff}}$ ), and it ranges from -0.33 to 0.19 in our sample, which is

not much different from the standard deviation ( $\sim 0.21$ ) in the fitting of  $\log g$  (see Fig. 9). As a result, we conclude that the dependence of  $[\text{Fe}/\text{H}]$  on  $\log g$  can be ignored. (This is consistent with what we found in Section 4.1; the role of metallicity is marginal in the WBR.)

The equation derived by Lutz & Pagel (1982) for stars with solar metallicity ( $-0.35 \leq [\text{Fe}/\text{H}] \leq 0.35$ ) is

$$\log W = -0.232 \log g + 1.78 \log T_{\text{eff}} - 4.15, \quad (4)$$

We can rearrange Eq. (4) to derive  $\log g$  as

$$\log g = -4.31 \log W + 7.67 \log T_{\text{eff}} - 17.9. \quad (5)$$

As noted above, the majority (86%) of our sources are close to solar metallicity, and even including the full sample, the dependence of  $\log g$  on  $[\text{Fe}/\text{H}]$  is very minor. Therefore, we can directly compare the Eq. (2) with Eq. (5). The mean difference in  $\log g$  between these two equations is  $\sim 0.31$ , applied across the full sample. Lutz & Pagel (1982) used low resolution spectral data and stellar atmospheric parameters from the literature; we have derived  $\log g$  of each sample star using a consistent detailed analysis with homogeneous high resolution spectral data. Therefore, we believe that the equation of gravity derived in this study is more robust.

### 5.3. Application to M Type Stars

In this study, only G and K type stars were used to determine the relationship among  $\log g$ ,  $\log T_{\text{eff}}$ , and  $\log W$  because of temperature limits in the Kurucz ATLAS9 model grids ( $T_{\text{eff}} \geq 3500$  K). In order to apply this relation to M type stars, the effective temperatures of M type stars need to be calculated by other methods. We applied the (V-K) color method to G and K stars, whose temperatures are derived using the stellar atmospheric model, and

found that the method works well. Following van Belle et al. (1999), we assume that the (V-K) color method is a reliable temperature indicator for M stars, as checked for G and K stars. With the derived  $T_{\text{eff}}$  and the measured width of the Ca II K emission line,  $\log g$  can be calculated for each M star based on the Eq. (2). The results are listed in Table 4. The calculated  $T_{\text{eff}}$  and  $\log g$  are comparable to the values found in other studies (Mallik 1998; Smith & Lambert 1986; Koleva & Vazdekis 2012). The difference between our calculations and the values reported in other studies is less than the standard deviation of  $\log g_{\text{fit}}$  ( $\sigma_{\log g, \text{fit}} = 0.21$ ). Therefore, we conclude that the relation determined in this study can be a useful tool to calculate the  $\log g$  of late-type stars without using stellar atmospheric models.

## 6. Summary

1. We derived the WBR ( $M_V = 33.76 - 18.08 \log W$ ) for 125 late-type stars, whose parallax errors are smaller than 10%, using high resolution echelle spectra obtained from BOES and UVES and visual magnitudes and parallaxes taken from the *Hipparcos* Catalogue.
2. Our WBR seems well-calibrated when compared to previous studies (Wallerstein et al. 1999; Pace et al. 2003).
3. We applied the WBR to M67 to calculate its distance modulus by using the spectra from Dupree et al. (1999). Our mean distance modulus from 5 stars agrees well with previous results. Therefore, we believe that our WBR is well-calibrated.
4. We determined the stellar atmospheric parameters ( $T_{\text{eff}}$ ,  $\log g$ ,  $[\text{Fe}/\text{H}]$ , and  $\xi_{\text{tur}}$ ) with a stellar model atmosphere (Kurucz ATLAS9) and an abundance analysis code (2010 version of MOOG). Using  $\log g$  and  $\log T_{\text{eff}}$  determined by the model, and the measurements of the Ca II K emission line width ( $\log W$ ), we found a relation of  $\log g_{\text{fit}} = - 5.85 \log W +$

$9.97 \log T_{\text{eff}} - 23.48$  with the standard deviation of 0.21 dex.

5. The surface gravities calculated with the above equation for 4 M type stars agree well with those values derived in previous studies within the standard deviation of  $\log g_{fit}$  ( $\sigma_{\log g, fit} = 0.21$ ). Therefore, this relation can provide a simple way to calculate the surface gravity of late-type stars without using stellar atmosphere models.

We are grateful to Dr. Dupree who kindly provided the M67 data. We also thank the anonymous referee for constructive comments and Dr. Green for English editing and clarity. This study was supported by the World Class University (WCU) program (No. R31-10016) and the Basic Science Research Program (No. 2012-0002330) through the National Research Foundation of Korea (NRF) funded by the Ministry of Education, Science and Technology (MEST) of the Korean government. This work was also supported by the Korea Astronomy and Space Science Institute (KASI) grant funded by the Korea government(MEST).

## REFERENCES

- Ayres, T. R. 1979, *ApJ*, 228, 509
- Bagnulo, S., Jehin, E., Ledoux, C., et al. 2003, *Msngr*, 114, 10
- Carraro, G., Girardi, L., Bressan, A., et al. 1996, *A&A*, 305, 849
- Casagrande, L., Ramirez, I., Melendez, J., et al. 2010, *A&A*, 512, 54
- Cox, N. L. J., Kaper, L., & Mokiem, M. R. 2005, *A&A*, 436, 661
- Cutri, R. M., Skrutskie, M. F., van Dyk, S., Beichman, C. A., Carpenter, J. M., et al. 2003, The 2MASS All-Sky Catalog of Point Sources. University of Massachusetts and Infrared Processing and Analysis Center (IPAC/California Institute of Technology).
- Dupree, A. K., & Smith, G. H. 1995, *AJ*, 110, 405
- Dupree, A. K., Whitney, B. A., Pasquini, L. 1999, *AJ*, 520, 751
- Gomez, T., Wallerstein, G., & Pancino, E. 2012, *PASP*, 124, 1246
- Kang, W., Lee, S. G., & Kim, K. M. 2011, *ApJ*, 736, 87
- Kang, W., & Lee, S. G. 2012, *MNRAS*, 425, 3162
- Koleva, M., & Vazdekis, A. 2012, *A&A*, 538, 143
- Kurucz R. L. 1993, CD-ROMs, ATLAS9 Stellar Atmospheres Programs and 2 km s<sup>-1</sup> Grid (Cambridge: Smithsonian Astrophys. Obs.)
- Lutz, T. E. 1970, *AJ*, 75, 1007
- Lutz, T. E. & Kelker, D. H. 1973, *PASP*, 85, 573
- Lutz, T. E. & Pagel, B. E. J. 1982, *MNRAS*, 199, 1101



- Mallik, S. V. 1998, *A&A*, 338, 623
- Montgomery, K. A., Marschall, L. A., & Janes, K. A. 1993, *AJ*, 106, 181
- Neckel, H. 1974, *A&A*, 35, 99
- Pace, G., Pasquini, L., & S. Ortolani 2003, *A&A*, 401, 997
- Pasquini, L., Brocato, E., & Pallavicini, R. 1990, *A&A*, 234, 277
- Pasquini, L. 1992, *A&A*, 266, 347
- Reimers, D. 1973, *A&A*, 24, 79
- Sanders, W. L. 1977, *A&AS*, 27, 89
- Sarajedini, A., Dotter, A., & Kirkpatrick, A. 2009, *ApJ*, 698, 1872
- Smith, V. V., & Lambert, D. L. 1986, *ApJ*, 311, 843
- Snedden C. 1973, Ph.D. Thesis, University of Texas
- van Belle, G. T., Lane, B. F., Thompson, R. R., et al. 1999, *AJ*, 117, 521
- van Leeuwen, F. 2007, *A&A*, 474, 653
- Wallerstein, G., Machado-Pelaez, L., & Gonzalez, G. 1999, *PASP*, 111, 335
- Wilson, O. C., & Bappu, M. K. V. 1957, *ApJ*, 125, 661
- Wilson, O. C. 1976, *ApJ*, 205, 823

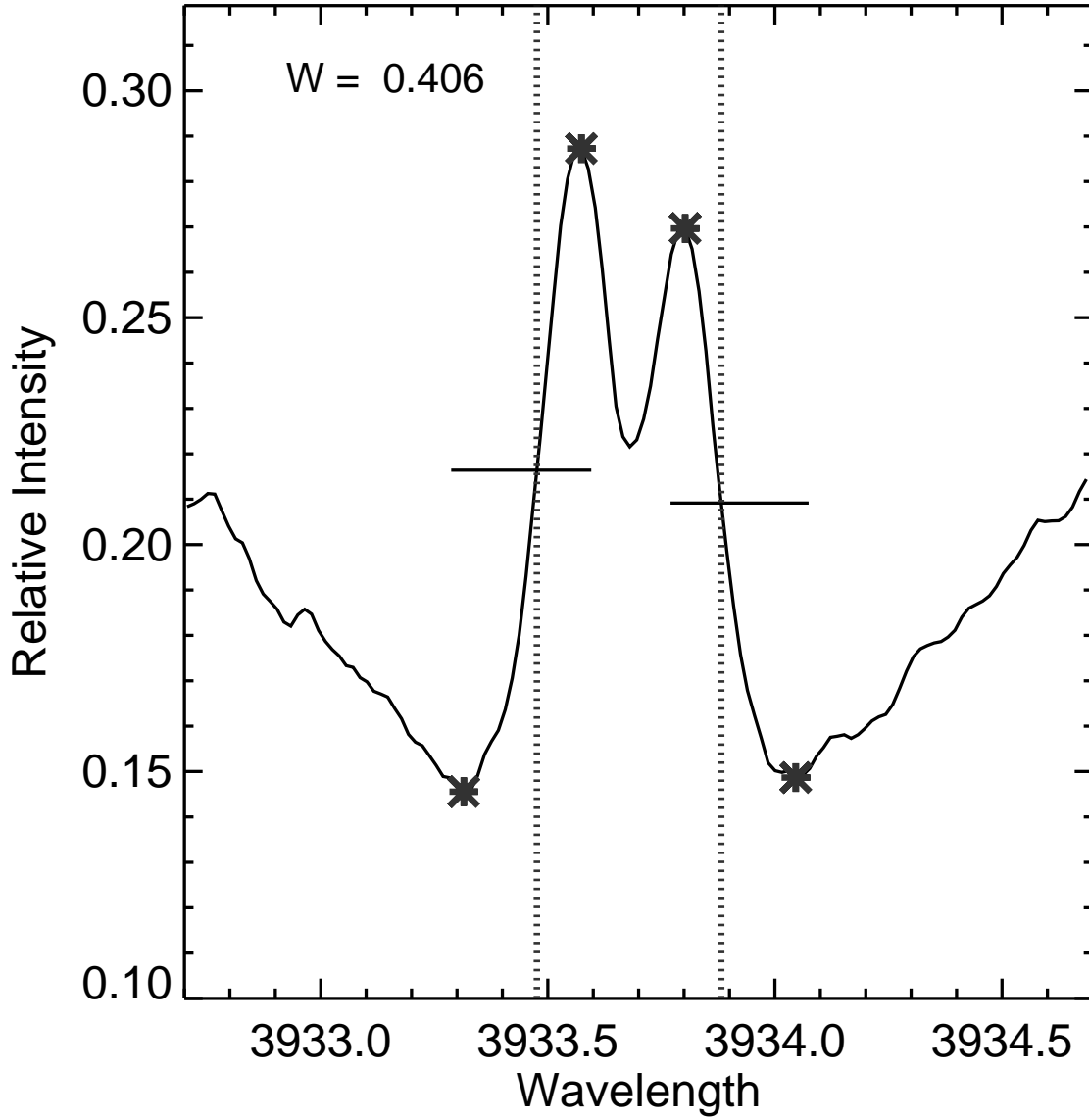


Fig. 1.— Measurement of Ca II K emission line widths. Asterisks mark the maximum and the minimum points of red and blue peaks. The difference between the two dashed lines represents the width of the Ca II K emission line ( $\log W$ ).

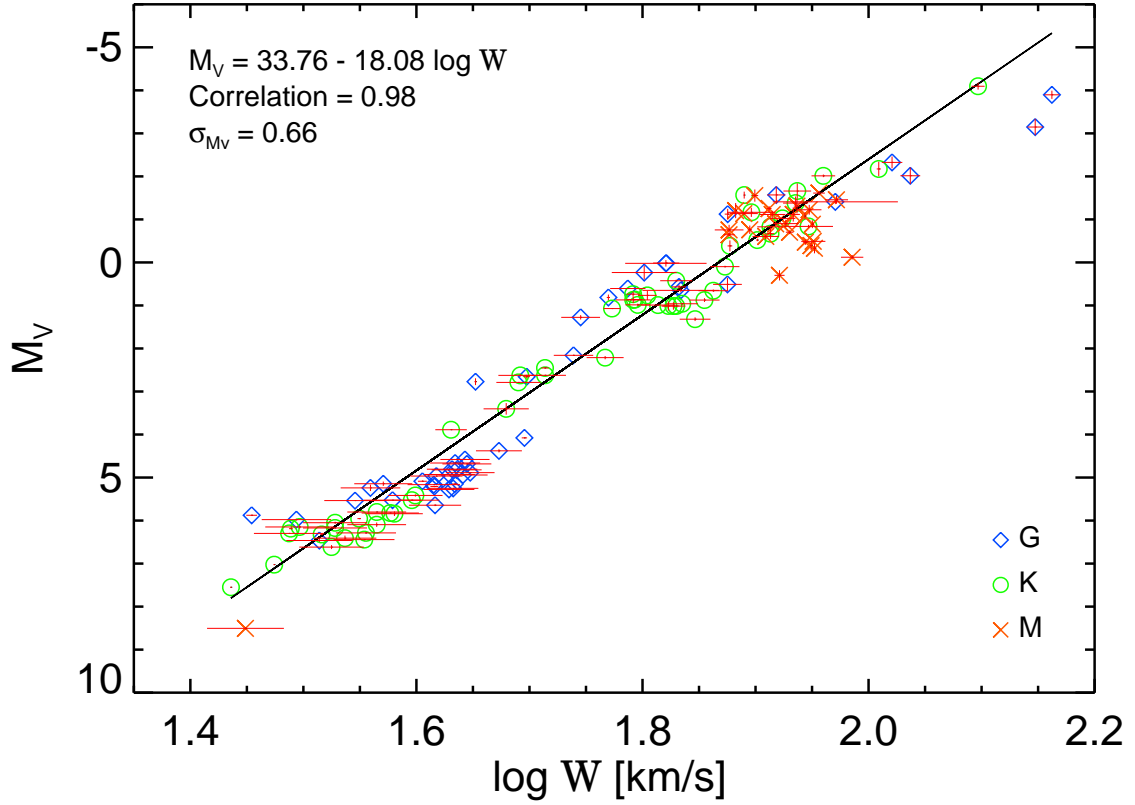


Fig. 2.— The Wilson-Bappu relation of our samples,  $M_V$  vs.  $\log W$ . The 125 stars with parallax errors less than 10% were used for fitting. The blue diamond, green circle, and orange cross symbols indicate G, K, and M type stars, respectively. The red error bars represent the errors of the measurements of  $\log W$  and  $M_V$  that originated from their parallax measurements.

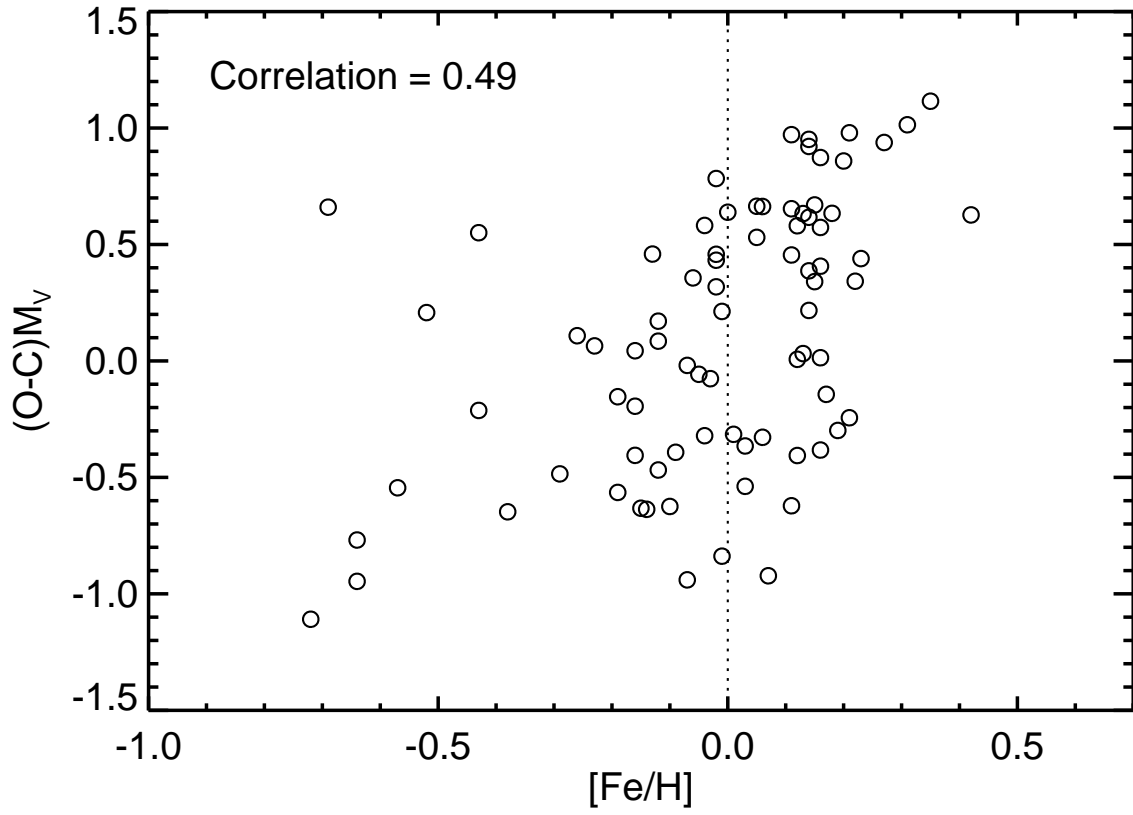


Fig. 3.—  $(O-C)M_V$  vs.  $[Fe/H]$ . The correlation coefficient between two quantities is 0.49. Dashed line represents the solar metallicity.

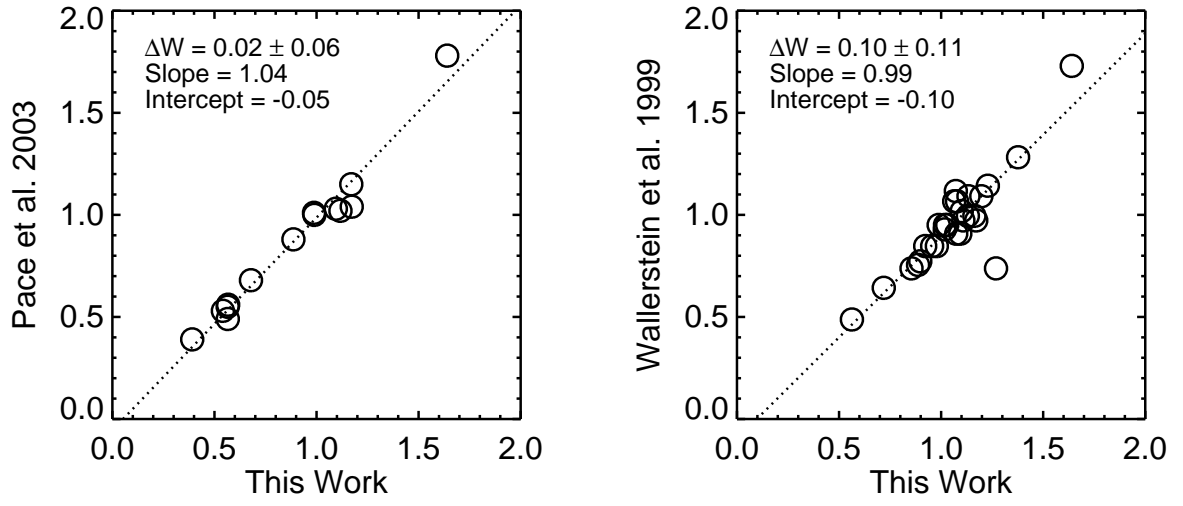


Fig. 4.— Comparisons with previous works for the width ( $W$  [ $\text{\AA}$ ]) of the Ca II K emission line: Pace et al. (2003) (left) and Wallerstein et al. (1999) (right).

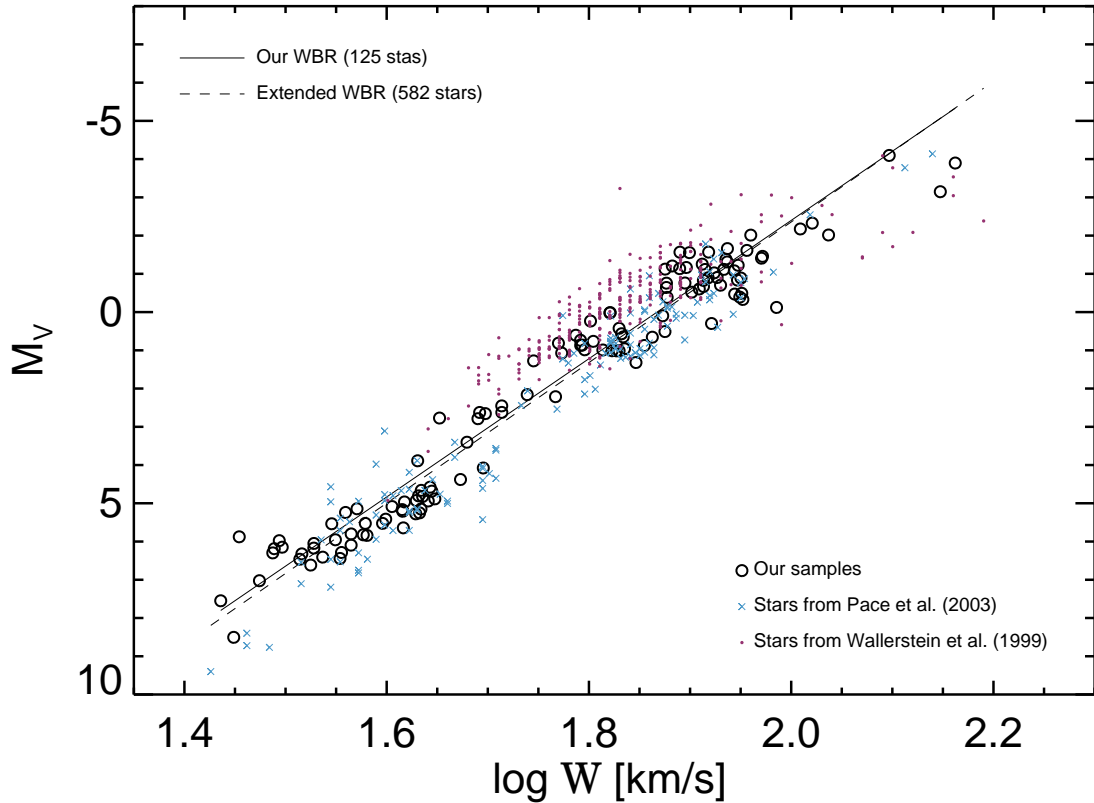


Fig. 5.— WBRs from extended and homogenised samples. Open circles indicate our sample (125 stars), blue crosses represent the stars from Pace et al. (2003) (131 stars), and purple filled circles correspond to the stars from Wallerstein et al. (1999) (326 stars). Solid line and dashed line represent our WBR of 125 stars ( $M_V = 33.76 - 18.08 \log W$ ) and the WBR ( $M_V = 34.41 - 18.38 \log W$ ) calculated from the combined sample (582 stars), respectively.

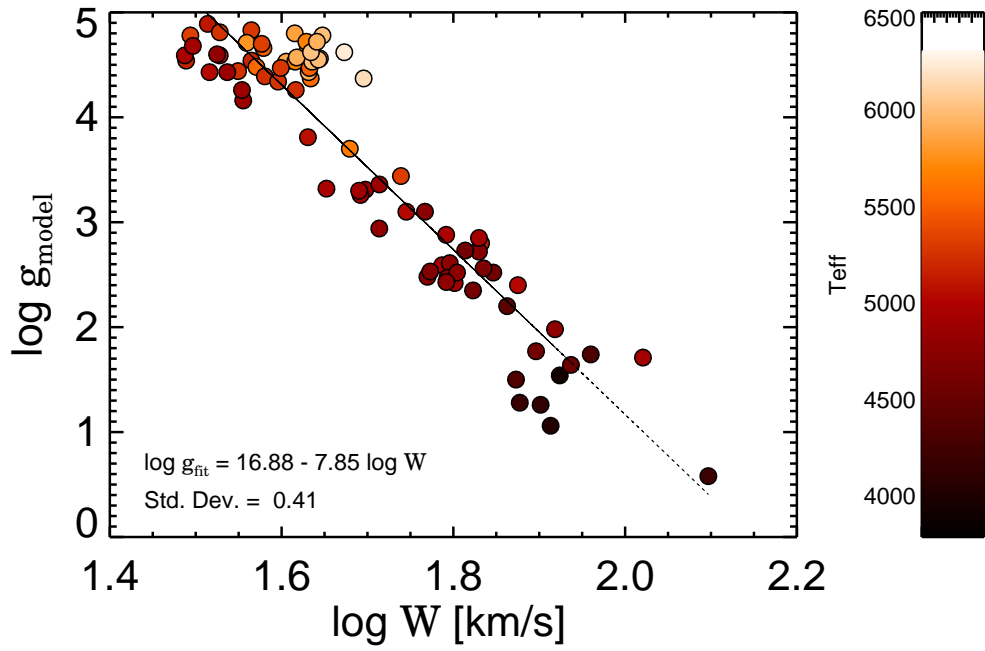


Fig. 6.— Plot of  $\log W$  vs.  $\log g_{\text{model}}$ . Color represents the effective temperature as determined by detailed analysis with model atmospheres. The standard deviation of  $\log g$  is 0.41.

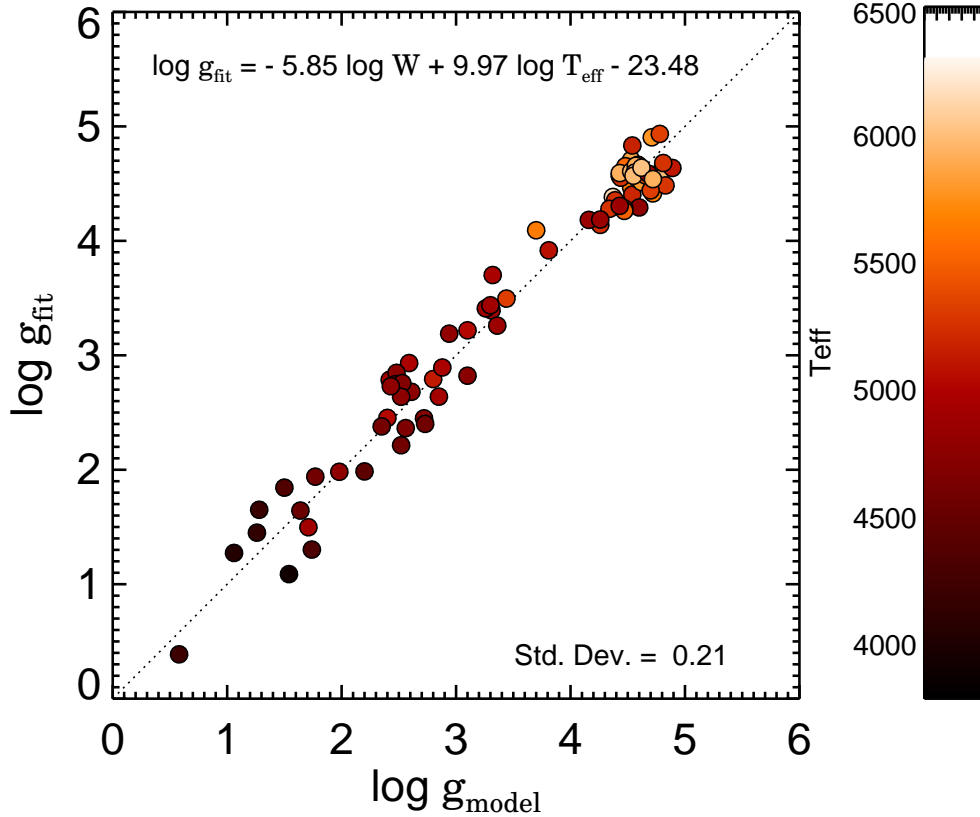


Fig. 7.— Plot of  $\log g_{\text{model}}$  vs.  $\log g_{\text{fit}}$ .  $\log g_{\text{model}}$  was derived from the stellar atmospheric model and  $\log g_{\text{fit}}$  was obtained from Eq. (2). Symbol color represents the effective temperature of the model atmosphere. The standard deviation in  $\log g$  is 0.21, which is smaller than that in Fig. 6.



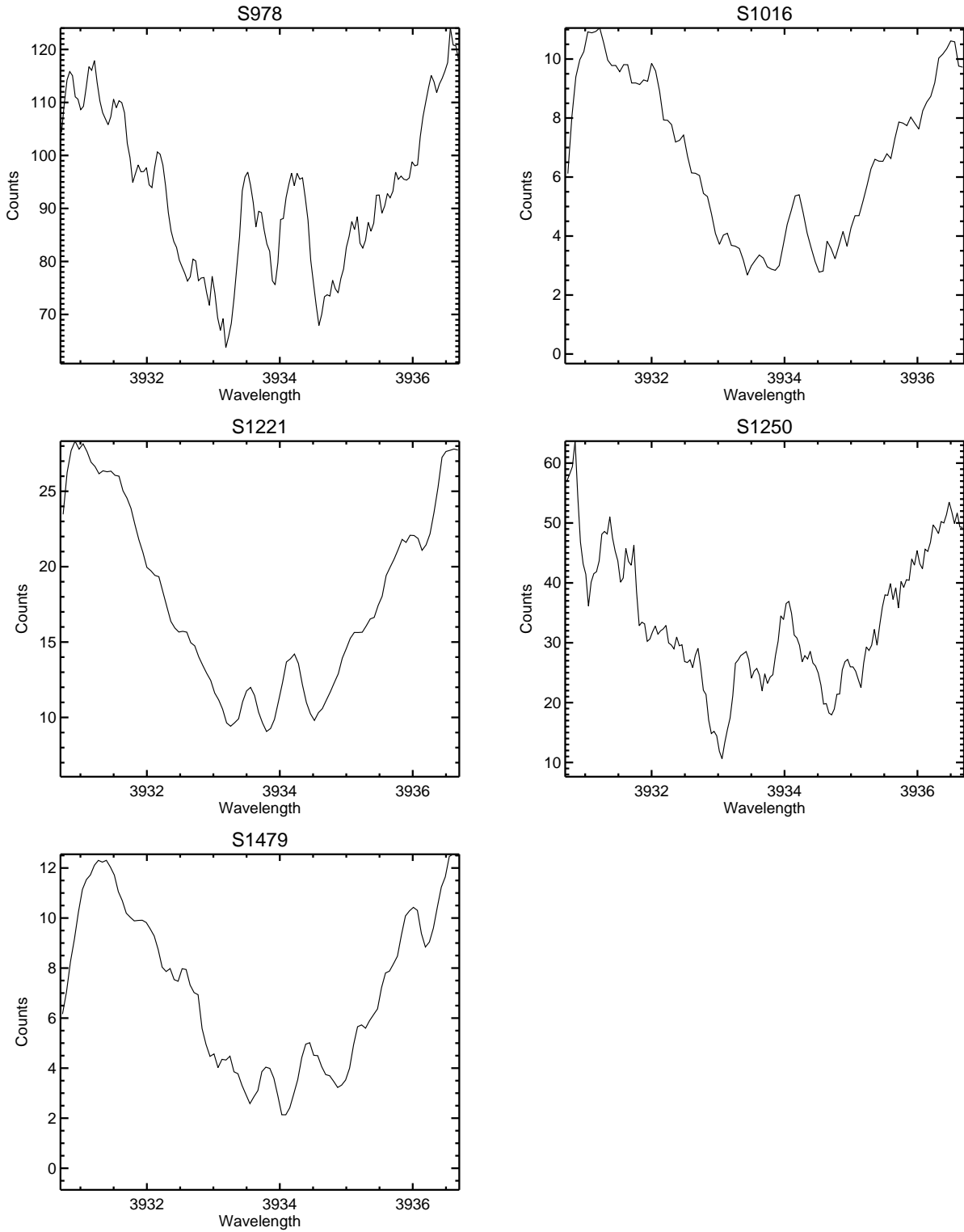


Fig. 8.— M67 spectra. Five spectra from Dupree et al. (1999) were used to determine the distance modulus to M67 (S978, S1016, S1221, S1250, S1479).

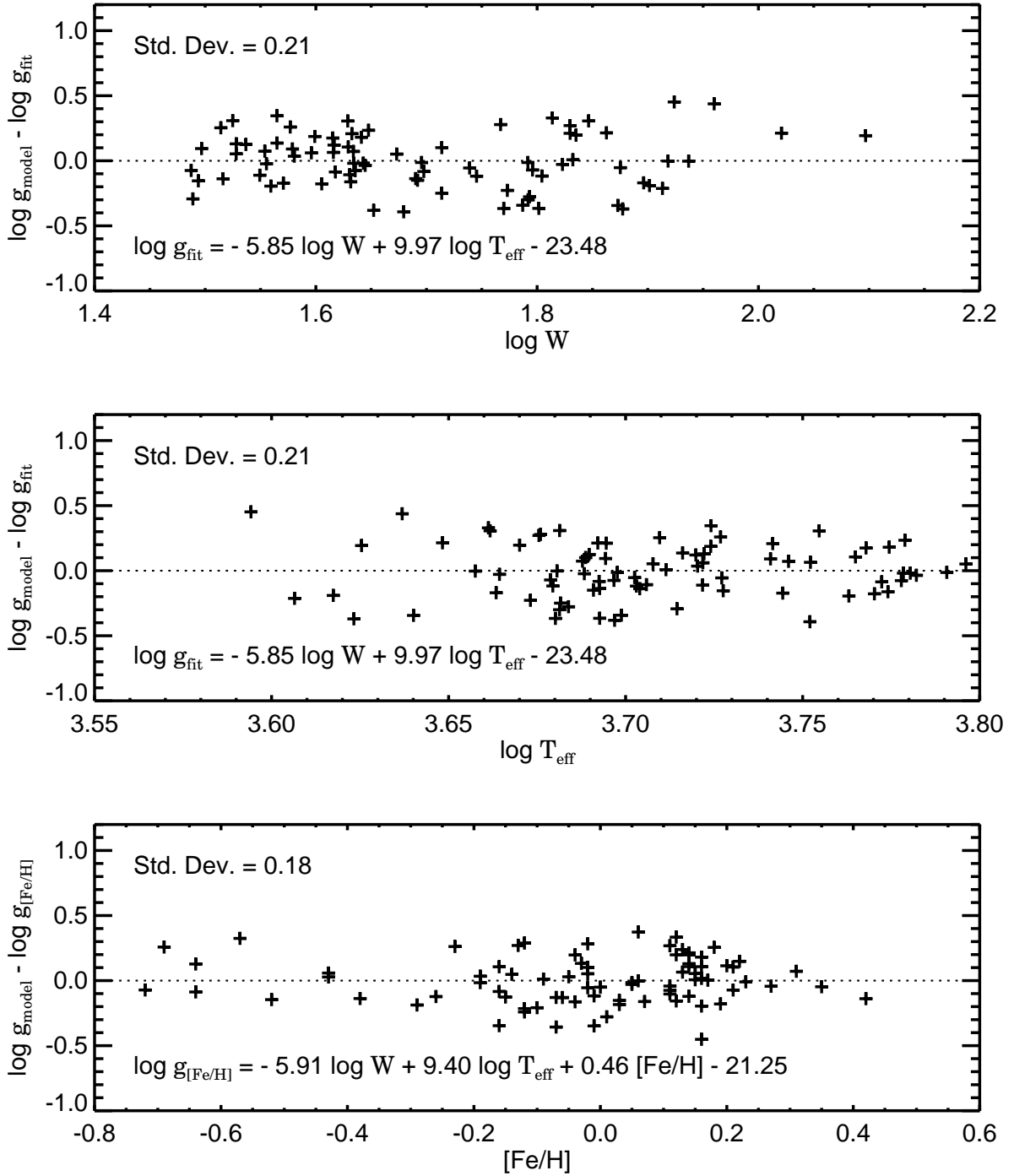


Fig. 9.— Surface gravity differences as a function of the width of the Ca II K emission line ( $\log W$ ), effective temperature ( $\log T_{\text{eff}}$ ), and metallicity ( $[\text{Fe}/\text{H}]$ ). The inclusion of  $[\text{Fe}/\text{H}]$  to  $\log g$  does not improve the fitting much.

Table 1. Our data sample

HD name	Sp.type <sup>b</sup>	V <sup>c</sup>	K <sup>d</sup>	Width	Werr	M <sub>V</sub>	M <sub>V</sub> err	T <sub>eff</sub>	log g	[Fe/H]	ξ <sub>tur</sub>	Instrument
		[mag]	[mag]	[Å]	[Å]	[mag]	[mag]	[K]	[dex]	[dex]	[km s <sup>-1</sup> ]	
HD3651 <sup>a</sup>	K0V	6.03	4.00	0.482	0.029	5.80	0.008	5201	4.54	0.15	0.73	BOES
HD7924 <sup>a</sup>	K0	7.31	5.16	0.443	0.029	6.17	0.017	5102	4.59	-0.16	0.36	BOES
HD11643	K1II	6.26	3.55	0.873	0.010	1.01	0.104	4617	2.35	0.14	1.51	UVES
HD11695	M4III	4.41	-0.77	1.117	0.008	-0.70	0.044	-	-	-	-	UVES
HD12642	M0III	5.73	1.75	1.167	0.003	-0.39	0.105	-	-	-	-	UVES
HD13974 <sup>a</sup>	G0V	4.98	3.08	0.562	0.029	4.81	0.009	5944	4.43	-0.43	0.33	BOES
HD20367 <sup>a</sup>	G0	6.52	5.04	0.618	0.029	4.38	0.037	6253	4.62	0.16	1.25	BOES
HD20630 <sup>a</sup>	G5Vv	4.98	2.96	0.541	0.029	5.17	0.006	5860	4.80	0.14	1.00	BOES
HD22049	K2Vk:	3.87	1.78	0.431	0.001	6.32	0.002	5058	4.43	-0.07	0.81	UVES
HD23249	K1III-IV	3.68	1.62	0.561	0.018	3.89	0.004	5080	3.81	0.16	0.88	UVES
HD24616	G8IV/V	6.83	4.55	0.589	0.001	2.77	0.079	4976	3.32	-0.72	1.05	UVES
HD25069	G9V	6.00	3.60	0.654	0.004	2.66	0.041	4926	3.31	0.12	1.14	UVES
HD25680 <sup>a</sup>	G5V	6.04	4.38	0.583	0.029	4.89	0.012	6010	4.78	0.14	1.02	BOES
HD27256	G8II-III	3.50	1.44	0.869	0.023	0.01	0.011	-	-	-	-	UVES
HD28305 <sup>a</sup>	K0III	3.70	1.42	0.887	0.029	0.43	0.024	4949	2.85	0.21	1.42	BOES
HD37124 <sup>a</sup>	G4IV-V	7.79	5.95	0.488	0.029	5.14	0.051	5551	4.48	-0.43	0.72	BOES
HD37811	G7III	5.60	3.36	0.868	0.072	0.02	0.076	-	-	-	-	UVES
HD39587 <sup>a</sup>	G0VCH-0.3	4.52	3.00	0.567	0.029	4.82	0.005	5996	4.53	0.00	1.00	BOES

Table 1—Continued

HD name	Sp.type <sup>b</sup>	V <sup>c</sup> [mag]	K <sup>d</sup> [mag]	Width [Å]	Werr [Å]	M <sub>V</sub> [mag]	M <sub>V</sub> err [mag]	T <sub>eff</sub> [K]	log g [dex]	[Fe/H] [dex]	ξ <sub>tur</sub> [km s <sup>-1</sup> ]	Instrument
HD42682	M2II-III	5.59	0.72	1.041	0.007	-1.55	0.142	-	-	-	-	UVES
HD45415	G9III	5.71	3.20	0.772	0.003	0.81	0.068	4788	2.48	-0.07	1.54	UVES
HD48329	G8Ib	3.19	0.12	1.906	0.029	-3.90	0.096	-	-	-	-	BOES
HD59967	G3V	6.79	5.10	0.529	0.005	5.09	0.018	5892	4.53	-0.06	1.26	UVES
HD65583 <sup>a</sup>	G8V	7.11	5.09	0.409	0.029	5.98	0.020	5340	4.78	-0.64	0.34	BOES
HD67594	G2Ib	4.52	2.32	1.843	0.029	-3.15	0.190	-	-	-	-	BOES <sup>†</sup>
HD72905 <sup>a</sup>	G1.5Vb	5.76	4.17	0.544	0.029	4.96	0.012	5920	4.57	-0.02	1.08	BOES <sup>†</sup>
HD74006	G7Ib-II	4.13	1.84	1.226	0.156	-1.41	0.053	-	-	-	-	UVES
HD75732 <sup>a</sup>	G8V	6.11	4.01	0.543	0.029	5.64	0.020	5246	4.26	0.35	0.89	BOES
HD76151 <sup>a</sup>	G3V	6.14	4.46	0.559	0.029	4.93	0.015	5820	4.62	0.13	0.96	BOES
HD76827	M3III	4.81	0.31	1.269	0.029	-0.12	0.052	-	-	-	-	BOES
HD77020	G9II	6.05	3.43	1.087	0.020	-1.57	0.200	4793	1.98	-0.14	2.06	UVES
HD77912	G8Iab:	4.73	2.40	1.377	0.029	-2.33	0.136	4922	1.71	-0.13	2.26	BOES
HD79354	K5III	5.40	1.42	1.131	0.029	-1.38	0.153	-	-	-	-	BOES
HD79452	G6III	6.14	3.86	0.984	0.029	0.51	0.152	5041	2.40	-0.69	1.57	BOES
HD81040 <sup>a</sup>	G0V	7.86	6.16	0.476	0.029	5.24	0.074	5795	4.71	-0.04	0.80	BOES
HD81146	K2III	4.62	1.69	0.956	0.029	0.66	0.028	4449	2.20	-0.04	1.51	BOES
HD81688 <sup>a</sup>	K0III-IV	5.56	3.06	0.812	0.029	0.87	0.073	4801	2.43	-0.29	1.47	BOES

Table 1—Continued

HD name	Sp.type <sup>b</sup>	V <sup>c</sup> [mag]	K <sup>d</sup> [mag]	Width [Å]	Werr [Å]	$M_V$ [mag]	$M_{V\text{-err}}$ [mag]	$T_{eff}$ [K]	$\log g$ [dex]	[Fe/H] [dex]	$\xi_{tur}$ [km s <sup>-1</sup> ]	Instrument
HD82210	G4III-IV	4.69	2.51	0.719	0.029	2.16	0.013	5335	3.44	-0.19	1.26	BOES
HD82885 <sup>a</sup>	G8IIIv	5.54	3.69	0.563	0.029	5.25	0.008	5515	4.47	0.31	1.06	BOES
HD83240	K1III	5.17	2.66	0.836	0.016	0.77	0.106	4780	2.52	0.03	1.39	UVES
HD84335	M3III	5.14	0.34	1.126	0.015	-1.12	0.166	-	-	-	-	BOES
HD89758	M0III	3.15	-1.01	1.078	0.029	-1.11	0.083	-	-	-	-	BOES
HD94600	K1III	5.19	2.33	0.939	0.029	0.87	0.044	-	-	-	-	BOES
HD95578	M0III	4.83	0.81	1.229	0.029	-1.46	0.093	-	-	-	-	BOES
HD99322	K0III	5.38	3.04	0.812	0.011	0.74	0.058	4985	2.88	0.11	1.34	UVES
HD99492 <sup>a</sup>	K2V	7.70	5.26	0.452	0.029	6.41	0.059	4894	4.43	0.23	0.76	BOES
HD99648	G8Iab:	5.12	2.83	0.985	0.006	-1.12	0.124	-	-	-	-	UVES
HD100029	M0III	3.92	-0.11	1.018	0.029	-1.14	0.033	-	-	-	-	BOES
HD100623	K0V	6.10	4.02	0.404	0.001	6.19	0.008	5182	4.54	-0.38	0.63	UVES
HD101153	M4III	5.22	-0.21	0.988	0.029	-0.76	0.119	-	-	-	-	BOES
HD101501 <sup>a</sup>	G8V	5.45	3.59	0.498	0.029	5.53	0.006	5507	4.66	-0.02	0.84	BOES
HD102195 <sup>a</sup>	K0V	8.21	6.15	0.499	0.029	5.84	0.054	5252	4.39	0.06	0.76	BOES
HD102212	M1III	4.14	0.16	0.988	0.011	-0.64	0.035	-	-	-	-	UVES
HD102224	K0.5IIIb	3.86	0.99	0.979	0.029	0.10	0.020	4366	1.50	-0.52	1.75	BOES
HD102328	K3III	5.43	2.63	0.922	0.029	1.32	0.043	4589	2.52	0.14	1.81	BOES

Table 1—Continued

HD name	Sp.type <sup>b</sup>	V <sup>c</sup> [mag]	K <sup>d</sup> [mag]	Width [Å]	Werr [Å]	M <sub>V</sub> [mag]	M <sub>V</sub> err [mag]	T <sub>eff</sub> [K]	log g [dex]	[Fe/H] [dex]	ξ <sub>tur</sub> [km s <sup>-1</sup> ]	Instrument
HD104304	G8IV	5.69	4.03	0.565	0.003	5.15	0.009	5572	4.37	0.27	0.97	UVES
HD107325	K2III-IV	5.69	3.10	0.767	0.029	2.21	0.038	4742	3.10	0.16	1.29	BOES
HD107446	K3.5III	3.73	0.31	1.046	0.002	-0.52	0.026	4144	1.26	-0.26	1.74	UVES
HD108225	G8III	5.18	2.86	0.895	0.070	0.65	0.044	-	-	-	-	BOES
HD108381	K1III	4.52	1.81	0.898	0.029	0.96	0.021	4678	2.56	0.14	1.64	BOES
HD110458	K0III	4.83	2.27	0.820	0.021	0.99	0.028	4773	2.61	0.19	1.46	UVES
HD110833 <sup>a</sup>	K3V	7.16	4.78	0.471	0.029	6.29	0.021	4879	4.16	0.11	0.36	BOES
HD111395 <sup>a</sup>	G5V	6.43	4.64	0.558	0.029	5.28	0.017	5684	4.72	0.11	0.88	BOES
HD112300	M3III	3.44	-1.19	1.172	0.029	-0.49	0.029	-	-	-	-	BOES
HD115383	G0V	5.31	4.03	0.651	0.004	4.08	0.010	6176	4.37	0.21	1.26	UVES
HD118203 <sup>a</sup>	K0	8.20	6.54	0.627	0.029	3.40	0.135	5650	3.70	0.16	1.01	BOES
HD119149	M1.5III	5.10	0.70	1.170	0.004	-0.89	0.092	-	-	-	-	UVES
HD120052	M2III	5.49	0.73	1.001	0.001	-1.20	0.176	-	-	-	-	UVES
HD120933	K5III	4.78	-0.01	1.019	0.001	-1.57	0.080	-	-	-	-	BOES
HD121416	K1III	5.98	3.44	0.882	0.022	1.01	0.087	-	-	-	-	UVES
HD123657	M4.5:III	5.10	-0.23	1.109	0.029	-0.90	0.089	-	-	-	-	BOES
HD123934	M1III	5.01	0.60	1.030	0.005	-0.76	0.098	-	-	-	-	UVES
HD130215 <sup>a</sup>	K2V	8.11	5.98	0.482	0.029	6.10	0.051	5298	4.83	0.18	0.90	BOES

Table 1—Continued

HD name	Sp.type <sup>b</sup>	V <sup>c</sup> [mag]	K <sup>d</sup> [mag]	Width [Å]	Werr [Å]	M <sub>V</sub> [mag]	M <sub>V</sub> err [mag]	T <sub>eff</sub> [K]	log g [dex]	[Fe/H] [dex]	ξ <sub>tur</sub> [km s <sup>-1</sup> ]	Instrument
HD130307 <sup>a</sup>	G8V	7.91	5.61	0.429	0.029	6.46	0.033	5124	4.89	-0.12	0.57	BOES
HD130328	M3III	5.72	-0.54	1.175	0.005	-0.33	0.118	-	-	-	-	UVES
HD130948 <sup>a</sup>	G1V	5.99	4.46	0.579	0.029	4.68	0.013	6055	4.56	0.05	1.07	BOES
HD131156	G8V	4.68	1.97	0.461	0.029	5.54	0.007	-	-	-	-	BOES
HD131511 <sup>a</sup>	K2V	6.14	4.32	0.495	0.029	5.82	0.012	5331	4.70	0.12	0.81	BOES
HD131873	K4III	2.20	1.29	1.074	0.029	-0.83	0.010	-	-	-	-	BOES
HD132813	M5III	4.58	-0.96	1.163	0.029	-1.22	0.114	-	-	-	-	BOES
HD135599 <sup>a</sup>	K0V	7.06	4.96	0.443	0.029	6.05	0.024	5274	4.81	-0.03	0.87	BOES
HD137759 <sup>a</sup>	K2III	3.46	0.67	0.855	0.029	0.99	0.007	4584	2.73	0.13	1.40	BOES
HD138716	K1IV	4.77	2.23	0.679	0.005	2.45	0.014	4804	2.94	0.01	1.24	UVES
HD140573	K2IIIb	2.80	0.15	0.887	0.006	1.01	0.009	4737	2.72	0.22	1.74	UVES
HD140901	G7IV	6.15	4.32	0.542	0.004	5.21	0.013	5652	4.53	0.15	0.80	UVES
HD145206	K4III	5.51	1.98	0.989	0.005	-0.38	0.128	4200	1.28	-0.16	1.66	UVES
HD145675 <sup>a</sup>	K0V	6.76	4.71	0.518	0.029	5.53	0.013	5270	4.34	0.42	0.67	BOES
HD147379	M1V	8.66	4.95	0.369	0.029	8.51	0.022	-	-	-	-	BOES
HD148291	K0II-IIICN	5.36	2.41	1.135	0.032	-1.66	0.178	4545	1.64	-0.09	2.05	UVES
HD148387	G8IIIb	2.87	0.58	0.803	0.029	0.61	0.006	4998	2.59	-0.01	1.38	BOES
HD148451	G5III	6.74	4.43	0.831	0.055	0.23	0.161	4928	2.42	-0.64	1.54	UVES

Table 1—Continued

HD name	Sp.type <sup>b</sup>	V <sup>c</sup> [mag]	K <sup>d</sup> [mag]	Width [Å]	Werr [Å]	M <sub>V</sub> [mag]	M <sub>V</sub> err [mag]	T <sub>eff</sub> [K]	log g [dex]	[Fe/H] [dex]	ξ <sub>tur</sub> [km s <sup>-1</sup> ]	Instrument
HD149447	K6III	4.28	0.39	1.161	0.058	-0.84	0.037	-	-	-	-	UVES
HD149661	K2V	5.91	4.04	0.465	0.002	5.95	0.008	5269	4.44	-0.01	1.00	UVES
HD156026	K5V	6.44	3.47	0.358	0.000	7.55	0.008	-	-	-	-	UVES
HD156274	G8V	5.61	3.42	0.373	0.004	5.88	0.013	-	-	-	-	UVES
HD156283	K3II	3.31	-0.02	1.197	0.029	-2.01	0.030	4334	1.74	0.06	2.08	BOES
HD156668 <sup>a</sup>	K2	8.57	6.00	0.439	0.029	6.62	0.046	4801	4.60	-0.02	0.44	BOES
HD160269 <sup>a</sup>	G0Va	5.35	3.74	0.577	0.029	4.58	0.011	6004	4.55	0.05	0.99	BOES
HD160346 <sup>a</sup>	K3V	6.66	4.10	0.470	0.029	6.44	0.016	4873	4.26	-0.02	0.69	BOES
HD164058	K5III	2.36	-1.16	1.101	0.029	-1.02	0.010	3928	1.54	0.12	1.84	BOES
HD164922 <sup>a</sup>	K0V	7.15	5.11	0.521	0.029	5.42	0.026	5297	4.47	0.16	0.60	BOES
HD166620 <sup>a</sup>	K2V	6.52	4.23	0.403	0.029	6.30	0.007	4974	4.59	-0.19	0.05	BOES
HD167042 <sup>a</sup>	K1III	6.14	3.55	0.645	0.029	2.63	0.028	4908	3.26	0.03	1.07	BOES
HD167818	K5III	4.78	0.82	1.340	0.006	-2.17	0.167	-	-	-	-	UVES
HD169916	K0IV	2.98	0.33	0.778	0.013	1.07	0.008	4711	2.53	-0.10	1.34	UVES
HD183255 <sup>a</sup>	K3V	8.15	5.57	0.412	0.029	6.15	0.040	4947	4.68	-0.57	0.62	BOES
HD188650	G1Ib-IIe	5.93	4.11	1.429	0.029	-2.02	0.192	-	-	-	-	BOES
HD189124	M6III	4.76	-1.53	1.153	0.000	-1.08	0.083	-	-	-	-	UVES
HD189763	M4III	4.45	-0.83	1.072	0.005	-1.25	0.054	-	-	-	-	UVES



Table 1—Continued

HD name	Sp.type <sup>b</sup>	V <sup>c</sup> [mag]	K <sup>d</sup> [mag]	Width [Å]	Werr [Å]	M <sub>V</sub> [mag]	M <sub>V</sub> err [mag]	T <sub>eff</sub> [K]	log g [dex]	[Fe/H] [dex]	ξ <sub>tur</sub> [km s <sup>-1</sup> ]	Instrument
HD190406 <sup>a</sup>	G0V	5.92	4.39	0.565	0.029	4.66	0.014	6031	4.62	0.11	0.88	BOES
HD190771 <sup>a</sup>	G5IV	6.32	4.62	0.574	0.029	4.94	0.015	5949	4.72	0.20	1.15	BOES
HD196171	K0III-IV	3.27	0.70	0.815	0.013	0.86	0.012	4829	2.47	-0.12	1.45	UVES
HD198149 <sup>a</sup>	K0IV	3.57	1.39	0.643	0.029	2.79	0.003	4928	3.30	-0.16	0.88	BOES
HD198357	K3II	5.67	2.27	1.075	0.008	-0.67	0.129	4041	1.06	-0.12	1.55	UVES
HD199665 <sup>a</sup>	G6III:	5.67	3.37	0.730	0.029	1.28	0.051	5047	3.10	0.07	1.18	BOES
HD199951	G6III	4.81	2.54	0.892	0.013	0.57	0.040	5145	2.80	-0.05	1.46	UVES
HD202320	K0II/III	5.33	2.52	1.033	0.051	-1.16	0.107	4607	1.77	-0.15	1.94	UVES
HD206778	K2Ib	2.55	-0.86	1.640	0.022	-4.10	0.078	4221	0.58	-0.23	2.89	UVES
HD209100	K5V	4.83	2.24	0.391	0.001	7.03	0.002	-	-	-	-	UVES
HD210066	M1III	5.12	1.62	1.154	0.006	-0.47	0.062	-	-	-	-	UVES
HD213080	M4.5IIIa	4.14	-0.91	1.086	0.000	-0.90	0.051	-	-	-	-	UVES
HD214665	M4III	5.12	-0.16	1.064	0.029	-0.60	0.072	-	-	-	-	BOES
HD214952	M5III	2.07	-3.32	1.186	0.014	-1.61	0.052	-	-	-	-	UVES
HD219215	M2III	4.32	-0.10	1.094	0.011	0.30	0.120	-	-	-	-	UVES
HD222404 <sup>a</sup>	K1IV	3.38	1.04	0.679	0.029	2.62	0.012	4883	3.36	0.17	1.11	BOES
HD224935	M3III	4.41	-0.40	1.134	0.007	-1.31	0.170	-	-	-	-	UVES

<sup>a</sup>These BOES data have been published by Kang et al. (2011).

<sup>b</sup>Spectral types are from the SIMBAD database.

<sup>c</sup>V magnitudes are taken from the *Hipparcos* Catalogue (van Leeuwen 2007).

<sup>d</sup>K magnitudes are taken from the 2MASS All-Sky Catalogue (Cutri et al. 2003).

Table 2. M67

Sanders ID <sup>a</sup>	Width [ $\text{\AA}$ ] <sup>b</sup>	Width [ $\text{\AA}$ ] Pace et al. (2003)	$m_V^c$	$M_V^d$	$(m - M)_V^e$	$(m - M)_V$ Pace et al. (2003)
S978	1.089	1.080	9.72	-0.936	10.656	10.926
S1016	0.804	0.700	10.30	1.446	8.854	8.116
S1221	0.894	0.854	10.76	0.613	10.147	10.131
S1250	0.953	0.997	9.69	0.111	9.579	10.271
S1479	0.908	0.868	10.55	0.491	10.059	10.048

<sup>a</sup>Sanders ID numbers were taken from Sanders (1977).

<sup>b</sup>Our measurement of the line width.

<sup>c</sup>The apparent magnitude from the *Hipparcos* Catalogue (van Leeuwen 2007).

<sup>d</sup>The absolute magnitude calculated by our WBR.

<sup>e</sup>The distance modulus calculated with c and d.

Table 3. Correction for the Lutz-Kelker effect

$\frac{\sigma_\pi}{\pi}$ <sup>a</sup>	$\Delta M$ <sup>b</sup>	Number of Stars
0.0	0.0	0
0.0 ~ 0.025	-0.01	81
0.025 ~ 0.050	-0.02	23
0.050 ~ 0.075	-0.06	13
0.075 ~ 0.100	-0.11	8

<sup>a</sup>The ratio of parallax error to parallax.

<sup>b</sup>The correction for the absolute magnitude from Lutz & Kelker (1973).

Table 4. Application to M type stars

HD name	Sp.type	$\log W$ [km s <sup>-1</sup> ]	$T_{\text{eff}}(\text{V-K})$ [K]	$\log g(\text{fit})$ [dex]	$T_{\text{eff}}(\text{ref.})$ [K]	$\log g(\text{ref.})$ [dex]
HD 89758	M0 III	1.92	3851.62	1.07	3700 <sup>a</sup>	1.35 <sup>a</sup>
HD 101153	M4 III	1.88	3464.98	0.83	3452 <sup>b</sup>	0.80 <sup>b</sup>
HD 102212	M1 III	1.88	3918.59	1.36	3738 <sup>c</sup>	1.55 <sup>c</sup>
HD 123657	M4.5 III	1.93	3484.12	0.56	3261 <sup>c</sup>	0.59 <sup>c</sup>

<sup>a</sup>Mallik (1998)

<sup>b</sup>Smith & Lambert (1986)

<sup>c</sup>Koleva & Vazdekis (2012)